BornAgain

Incomplete Physics Manual

Software version 1.16

This document last updated March 29, 2020

Marina Ganeva, Gennady Pospelov, Walter Van Herck, Joachim Wuttke

Scientific Computing Group
Jülich Centre for Neutron Science
at Heinz Maier-Leibnitz Zentrum Garching
Forschungszentrum Jülich GmbH

Homepage: http://www.bornagainproject.org

Authors: Marina Ganeva, Gennady Pospelov, Walter Van Herck, Joachim Wuttke

Scientific Computing Group

at Heinz Maier-Leibnitz Zentrum (MLZ) Garching

Disclaimer: Software and documentation are work in progress.

We cannot guarantee correctness and accuracy.

If in doubt, contact us for assistance or scientific collaboration.

Funding: This project has received funding from the European Union's Horizon 2020 research and innovation programme under grant agreement No 654000.

Contents

Preface

About BornAgain

BornAgain is a software package to simulate and fit reflectometry, off-specular scattering, and grazing-incidence small-angle scattering (GISAS) of X-rays and neutrons. It provides a generic framework for modeling multilayer samples with smooth or rough interfaces and with various types of embedded nanoparticles. The name, BornAgain, alludes to the central role of the distorted-wave Born approximation (DWBA) in the physical description of the scattering process.

BornAgain is maintained by the Scientific Computing Group of the Jülich Centre for Neutron Science (JCNS) at Heinz Maier-Leibnitz Zentrum (MLZ) Garching, Germany. It free and open source software. The source code is released under the GNU General Public License (GPL, version 3 or higher), the documentation under the Creative Commons license CC-BY-SA.

This manual vs other documentation

This Physics Manual explains some of the theory behind BornAgain. It is restricted to topics that are not covered by other components of the BornAgain documentation. These include:

- Our 2020 article in J. Appl. Cryst. [1] that gives a broad overview over BornAgain. The implemented physics is summarized in Sect. 5.
- The web site `https://www.bornagainproject.org`, which includes instructions how to download and install BornAgain, and extensive tutorials on setting up physical models.
- The complete documentation of the Application Programming Interface (API), which can be generated by running the open-source tool *Doxygen* over the source code.
- Further technical documents, available from the *Documents* tab on the download page. So far, there exists one such document, namely the Form factor catalog.

This Physics Manual is work in progress. In future editions, it may grow as we elaborate details or add new chapters, but it may also shrink as we move contents to journal articles or other documents.

Citation

The canonical reference for BornAgain is the journal article [1]

> Gennady Pospelov, Walter Van Herck, Jan Burle, Juan M. Carmona Loaiza, Céline Durniak, Jonathan M. Fisher, Marina Ganeva, Dmitry Yurov and Joachim Wuttke:
> BornAgain: software for simulating and fitting grazing-incidence small-angle scattering
> J. Appl. Cryst. 53, 262–276 (2020)

Use of the software should additionally be documented by citing a specific version thereof:

> BornAgain — Software for simulating and fitting X-ray and neutron small-angle scattering at grazing incidence, version ⟨`version`⟩ (⟨`release date`⟩), `http://www.bornagainproject.org`

Citation of the present Physics Manual is only necessary when referring to specific information. As this document is subject to frequent and substantial change, it is important to refer to a specific edition by indicating the release date printed on the title page:

> Marina Ganeva, Gennady Pospelov, Walter Van Herck, Joachim Wuttke:
> BornAgain Physics Manual (⟨`release date`⟩),
> `http://www.bornagainproject.org`

Old editions can be retrieved from the BornAgain source repository.

The initial design of BornAgain and much of the implemented physics owe much to the widely used program IsGISAXS by Rémi Lazzari [2]. Depending on how BornAgain is used in scientific work, it may be appropriate to cite the pioneering papers by Lazzari *et al.* [3, 4].

Typographic Conventions

We use the following colored boxes to highlight certain information:

Such a box contains a **warning** about potential problems with the software or the documentation.

This road sign in the margin indicates **work in progress**.

An **implementation note** explains how the theory exposed in this manual is actually used in BornAgain.

This is a link.

Mathematical notations are explained in the symbol index, page Y:1. Snomencl

This document is formatted for single-sided printing, which is more convenient for reading on a screen.

1 Scattering

This chapter provides a self-contained introduction into the theory of neutron and X-ray scattering, as needed for the analysis of grazing-incidence small-angle scattering (GISAS) experiments. In Section 1.1, a generic wave equation is derived. In Section 1.2, it is solved in first-order distorted-wave Born approximation (DWBA). The chapter finishes with a qualitative discussion of coherence lengths in Section 1.3.

1.1 Wave propagation

In this section, we review the wave equations that describe the propagation of neutrons (Secs. 1.1.1 and 1.1.2) and X-rays (Sec. 1.1.3) in matter, and combine them into a unified wave equation (Sec. 1.1.4) that is the base for the all following analysis. This provides justification and background for Eqns. 1–3 in the BornAgain reference paper [1].

1.1.1 Neutrons in a scalar potential

The scalar wavefunction $\psi(\boldsymbol{r},t)$ of a free neutron in absence of a magnetic field is governed by the Schrödinger equation

$$i\hbar\partial_t\psi(\boldsymbol{r},t) = \left[-\frac{\hbar^2}{2m}\boldsymbol{\nabla}^2 + V(\boldsymbol{r})\right]\psi(\boldsymbol{r},t). \tag{1.1}$$ {ESchrodi1}

Since BornAgain only aims at modelling elastic scattering, any time dependence of the potential is averaged out in the definition $V(\boldsymbol{r}) \coloneqq \langle V(\boldsymbol{r},t)\rangle$. Inelastic scattering, in principle, can be accounted for by an extra contribution damping.[1] Therefore we only need to consider monochromatic waves with given frequency ω. In consequence, the wavefunction

$$\psi(\boldsymbol{r},t) = \psi(\boldsymbol{r})\mathrm{e}^{-i\omega t} \tag{1.2}$$ {Estationarywave}

factorizes into a stationary wave and a time-dependent phase factor. In the following, we will characterize the incoming radiation not by its energy $\hbar\omega$, but by its *vacuum wavenumber* K, given by the dispersion relation

$$\hbar\omega = \frac{(\hbar K)^2}{2m}. \tag{1.3}$$

[1] This is not explicitly supported in the software, but users are free to increase the imaginary part of the refractive index to emulate damping by inelastic losses.

We shall use Fermi's pseudopotential in the rescaled form[2]

$$v(\boldsymbol{r}) \coloneqq \frac{2m}{\hbar^2} V(\boldsymbol{r}) = 4\pi \sum_j \langle b_j \delta\left(\boldsymbol{r} - \boldsymbol{r}_j(t)\right)\rangle \,. \tag{1.4}$$ {Evrard21}

The Schrödinger equation (1.1) then takes the simple form

$$\left[\boldsymbol{\nabla}^2 + K^2 - v(\boldsymbol{r})\right] \psi(\boldsymbol{r}) = 0. \tag{1.5}$$ {ESchrodi2}

The sum runs over all nuclei exposed to ψ. The *bound scattering length* b_j is isotope specific; values are tabulated [5]. Sea92

In small-angle scattering, as elsewhere in neutron optics [6], Sea89 the potential can be coarse-grained by spatially averaging over at least a few atomic diameters,

$$v(\boldsymbol{r}) = \sum_s b_s \rho_s(\boldsymbol{r}), \tag{1.6}$$ {Evrard21}

where the sum now runs over chemical elements, $b_s \coloneqq \langle b_j \rangle_{j \in s}$ is the bound *coherent* scattering length, and ρ_s is a number density. In passing from (1.4) to (1.6), we neglected Bragg scattering from atomic-scale correlation, and incoherent scattering from spin or isotope related fluctuations of b_j. In small-angle experiments, these types of scattering only matter as loss channels.[3] Furthermore, incoherent scattering, as inelastic scattering, contributes to the diffuse background in the detector. In conclusion, the coarse-grained neutron optical potential (1.6) is just a *scattering length density* (SLD) [6, eq. 2.8.37]. Sea89

1.1.2 Neutrons in a magnetic field

In presence of a magnetic field, the propagation of free neutrons becomes spin dependent. Therefore the scalar wavefunction of Sec. 1.1.1 must be replaced by spinor $\boldsymbol{\Psi}$. The magnetic moment μ of the neutron couples to the magnetic induction $\boldsymbol{B}$ [7, 8]. Mez86,MaOB06 With the coupling term, the Schrödinger equation (1.1) becomes

$$\left[-\frac{\hbar^2}{2m}\boldsymbol{\nabla}^2 + V(\boldsymbol{r}) + \mu \boldsymbol{B}(\boldsymbol{r})\hat{\boldsymbol{\sigma}} - \hbar\omega\right] \boldsymbol{\Psi}(\boldsymbol{r}) = 0, \tag{1.7}$$ {EHSchrodi}

where μ_0 is the vacuum permeability, and $\hat{\boldsymbol{\sigma}}$ is the Pauli vector, composed of the three Pauli matrices. We introduce the reduced field

$$\boldsymbol{b} \coloneqq \frac{2m\mu_0\mu_\mathrm{n}}{\hbar^2}\boldsymbol{B}, \tag{1.8}$$

to rewrite the Schrödinger equation in analogy to (1.5) as

$$\left[\boldsymbol{\nabla}^2 + K^2 - v(\boldsymbol{r}) - \boldsymbol{b}(\boldsymbol{r})\hat{\boldsymbol{\sigma}}\right] \boldsymbol{\Psi}(\boldsymbol{r}) = 0. \tag{1.9}$$ {ESchrodi2H}

[2] From here on, our notation differs by a factor of 4π from that in our 2020 paper [1]. PoHB20

[3] Same remark as in Footnote 1: To model these losses, use the imaginary part of the refractive index.

1.1.3 X-rays

The propagation of X-rays is governed by Maxwell's equations, which read in SI units

$$\begin{aligned} \boldsymbol{\nabla} \times \boldsymbol{E} &= -\partial_t \boldsymbol{B}, \quad \boldsymbol{\nabla} \boldsymbol{B} = 0, \quad \boldsymbol{B} = \boldsymbol{\mu}(\boldsymbol{r}) \mu_0 \boldsymbol{H}, \\ \boldsymbol{\nabla} \times \boldsymbol{H} &= +\partial_t \boldsymbol{D}, \quad \boldsymbol{\nabla} \boldsymbol{D} = 0, \quad \boldsymbol{D} = \boldsymbol{\epsilon}(\boldsymbol{r}) \epsilon_0 \boldsymbol{E}. \end{aligned} \tag{1.10}$$

{EMaxwell}

Since BornAgain only addresses elastic scattering, we assume the permeability and permittivity tensors $\boldsymbol{\mu}$ and $\boldsymbol{\epsilon}$ to be time-independent. Therefore, as in Sec. 1.1.1, we only need to consider monochromatic waves with given frequency ω, and each of the fields $\boldsymbol{E}$, $\boldsymbol{D}$, $\boldsymbol{H}$, $\boldsymbol{B}$ factorizes into a stationary field and a time-dependent phase factor.[4] We will formulate the following in terms of the electric field

$$\boldsymbol{E}(\boldsymbol{r}, t) = \boldsymbol{E}(\boldsymbol{r}) \mathrm{e}^{-i\omega t}. \tag{1.11}$$

{EstationaryX}

The other three fields can be obtained from $\boldsymbol{E}$ by straightforward application of (1.10).

Since magnetic refraction or scattering is beyond the scope of BornAgain, the relative magnetic permeability tensor is always $\boldsymbol{\mu}(\boldsymbol{r}) = 1$. As customary in SAXS and GISAXS, we assume that the dielectric properties of the material are those of a polarizable electron cloud.[5] Thereby the relative dielectric permittivity tensor $\boldsymbol{\epsilon}$ becomes a scalar,

$$\epsilon(\boldsymbol{r}) = 1 - \frac{4\pi r_e}{K^2} \rho(\boldsymbol{r}), \tag{1.12}$$

with the classical electron radius $r_e = e^2/(4\pi\epsilon_0 m c^2) \simeq 2.8 \cdot 10^{-15}$ m, the electron number density $\rho(\boldsymbol{r})$, and the vacuum wavenumber K, given by the dispersion relation

$$K^2 = \mu_0 \epsilon_0 \omega^2 = \omega^2 / c^2. \tag{1.13}$$

With these simplifying assumptions about $\boldsymbol{\epsilon}$ and $\boldsymbol{\mu}$, Maxwell's equations yield the wave equation

$$\boldsymbol{\nabla} \times \boldsymbol{\nabla} \times \boldsymbol{E} = K^2 \epsilon(\boldsymbol{r}) \boldsymbol{E}. \tag{1.14}$$

{ENabCrossNabE}

Using a standard identity from vector analysis, it can be brought into the more tractable form

$$\left[\boldsymbol{\nabla}^2 - \boldsymbol{\nabla} \cdot \boldsymbol{\nabla} + K^2 \epsilon(\boldsymbol{r})\right] \boldsymbol{E}(\boldsymbol{r}) = 0. \tag{1.15}$$

{ENabNabE}

[4] This phase factor can be defined with a plus or a minus sign in the exponent. Most texts on X-ray crystallography, including influential texts on GISAXS [4], prefer the *crystallographic convention* with a plus sign. In BornAgain, we prefer the opposite *quantum-mechanical convention* for consistency with the neutron case (1.2), where the minus sign is an inevitable consequence of the standard form of the Schrödinger equation.

ReLLOS

[5] This is occasionally called the *Laue model* [9].

Lau31

1.1.4 Unified wave equation

We combine all the above in a unified wave equation

$$[\boldsymbol{D}_0 - \boldsymbol{V}(\boldsymbol{r})]\,\boldsymbol{\Psi}(\boldsymbol{r}) = 0 \tag{1.16}$$ {EWAVE}

with the vacuum wave operator

$$\boldsymbol{D}_0 \coloneqq \begin{cases} \boldsymbol{\nabla}^2 + K^2 & \text{for neutrons,} \\ \boldsymbol{\nabla}^2 - \boldsymbol{\nabla}\cdot\boldsymbol{\nabla} + K^2 & \text{for X-rays} \end{cases} \tag{1.17}$$ {EDo}

and the potential

$$\boldsymbol{V}(\boldsymbol{r}) \coloneqq \begin{cases} v(\boldsymbol{r}) & \text{for neutrons (scalar),} \\ v(\boldsymbol{r}) + \boldsymbol{b}(\boldsymbol{r})\hat{\boldsymbol{\sigma}} & \text{for neutrons (spinorial),} \\ K^2(\epsilon(\boldsymbol{r}) - 1) & \text{for X-rays.} \end{cases} \tag{1.18}$$ {ETV}

The generic wave amplitude $\boldsymbol{\Psi}$ shall represent the scalar neutron wavefunction ψ, the spinor $\boldsymbol{\Psi}$, or the electric vector field $\boldsymbol{E}$, as applicable.

1.1.5 Density operator, flux

An eigenfunction of the vacuum wave operator $\boldsymbol{D}_0$ is a plane wave with real wavevector $\boldsymbol{k}$. In the spinor or vector case, its polarization shall be expressed in an orthonormal base $\{\boldsymbol{u}_\alpha\}$ with $\alpha = 1, 2$ (for spin 1/2 or for traverse electric field in vacuum). The corresponding eigenstate can be written as ket $|\boldsymbol{k}\alpha\rangle$, the real-space coordinate representation as

$$\boldsymbol{\Psi}_{\boldsymbol{k}\alpha}(\boldsymbol{r}) \equiv \langle \boldsymbol{r}|\boldsymbol{k}\alpha\rangle = (2\pi)^{-3/2}\boldsymbol{u}_\alpha \mathrm{e}^{i\boldsymbol{k}\boldsymbol{r}}. \tag{1.19}$$

The incident neutron beam in an actual scattering experiment is not such a *pure* state, but a statistical mixture of states, and must therefore be described by the density operator

$$\boldsymbol{\rho} \coloneqq \sum_{\boldsymbol{k}\alpha} p_{\boldsymbol{k}\alpha}\,|\boldsymbol{k}\alpha\rangle\,\langle\boldsymbol{k}\alpha|\,, \tag{1.20}$$ {EdefRho}

where $p_{\boldsymbol{k}\alpha}$ quantifies the contribution of pure state $|\boldsymbol{k}\alpha\rangle$.

In quantum mechanics, the current density, or flux, is measured by the operator

$$\boldsymbol{J} \coloneqq \frac{1}{2}\big[\,|\boldsymbol{r}\rangle\,\langle\boldsymbol{r}|\,\boldsymbol{k} + \boldsymbol{k}\,|\boldsymbol{r}\rangle\,\langle\boldsymbol{r}|\,\big]. \tag{1.21}$$ {EdefJop}

With (1.20), we obtain

$$\boldsymbol{J}(\boldsymbol{r}) \coloneqq \mathrm{Tr}(\boldsymbol{\rho}\boldsymbol{J}) = \sum_{\boldsymbol{k}\alpha} p_{\boldsymbol{k}\alpha}\,\mathrm{Re}(\boldsymbol{k})\,|\boldsymbol{\Psi}_{\boldsymbol{k}\alpha}|^2. \tag{1.22}$$ {EJ}

In the electromagnetic case, the energy flux is given by the Poynting vector, which for complex fields takes the form

$$\boldsymbol{S} \coloneqq \mathrm{Re}(\boldsymbol{E}(\boldsymbol{r},t)) \times \mathrm{Re}(\boldsymbol{H}(\boldsymbol{r},t)). \tag{1.23}$$

For a stationary plane wave $\boldsymbol{E}(\boldsymbol{r}) = \boldsymbol{E_k} \mathrm{e}^{i\boldsymbol{kr}}$ in vacuum, we find

$$S = \frac{1}{2\omega\mu_0} |\boldsymbol{E_k}|^2 \,\mathrm{Re}\,\boldsymbol{k}, \tag{1.24}$$

which confirms the common knowledge that the radiation intensity counted in a detector is proportional to the squared electric field amplitude. At constant frequency, the prefactor is ignorable so that we can use the quantum-mechanical flux (1.22) also for x-rays.

1.2 Distorted-wave Born approximation

To describe scattering from a condensed-matter sample, the wave equation is solved through a perturbation expansion. The ordinary form of this expansion, the *Born approximation* (BA), is derived in many textbooks.[6] For scattering under grazing-incidence, however, the more generic *distorted-wave Born approximation* (DWBA)[7] is required. In this section, we provide a self-contained derivation based on the unified neutron and X-ray wave equation (1.16).

1.2.1 Distortion versus perturbation

To get started, we decompose the potential (1.18) into a more regular and a more fluctuating part:

$$\boldsymbol{V}(\boldsymbol{r}) =: \boldsymbol{\Lambda}(\boldsymbol{r}) + \boldsymbol{U}(\boldsymbol{r}). \tag{1.25}$$ {Edecompose}

The *distortion field* $\boldsymbol{\Lambda}$ comprises regular, well-known features of the sample. The *perturbation potential* $\boldsymbol{U}$ stands for the more irregular, unknown features of the sample one ultimately wants to study in a scattering experiment. This is vague, and in certain situations the decomposition (1.25) is indeed to some extent arbitrary. However, in most practical cases $\boldsymbol{\Lambda}$ and $\boldsymbol{U}$ are clearly determined by the following basic idea of DWBA:

Only $\boldsymbol{U}$ shall be treated as a perturbation. The propagation of incident and scattered waves under the influence of $\boldsymbol{\Lambda}$, in contrast, shall be handled exactly, through analytical solution of the unperturbed distorted wave equation

$$\boldsymbol{D}(\boldsymbol{r})\boldsymbol{\Phi}(\boldsymbol{r}) = 0 \tag{1.26}$$ {EDPsi0}

with the *distorted wave operator*

$$\boldsymbol{D}(\boldsymbol{r}) \coloneqq \boldsymbol{D}_0 - \boldsymbol{\Lambda}(\boldsymbol{r}). \tag{1.27}$$

The solutions $\boldsymbol{\Phi}$ are the *distorted* waves that are the base of the distorted-wave Born approximation (DWBA), as developed below in Sect. 1.2.3. SxDWBA

[6] For a particularly detailed derivation see Schober's lecture notes on neutron scattering [10]. Sch14

[7] The DWBA was originally devised by Massey and Mott (ca 1933) for collisions of charged particles. Summaries can be found in some quantum mechanics textbooks (Messiah, Schiff) and in monographs on scattering theory (e. g. Newton). The first explicit applications to grazing-incidence scattering were published in 1982: Vineyard [11] discussed X-ray scattering, but failed to account for the distortion of the scattered wave; Mazur and Mills [12] deployed heavy formalism to compute the inelastic neutron scattering cross section of ferromagnetic surface spin waves from scratch. A concise derivation of the DWBA cross section was provided by Dietrich and Wagner (1984/85) for X-rays [13] and neutrons [14]. Unfortunately, their work was overlooked in much of the later literature, which often fell back to less convincing derivations. Vin82 MaMi82 Diwa84 Diwa85

1.2.2 Refractive index

Except for neutrons in a magnetic field the distortion field is scalar so that it can be expressed through the *refractive index*

$$n(\boldsymbol{r}) \coloneqq \sqrt{1-\frac{4\pi\Lambda(\boldsymbol{r})}{K^2}} = \begin{cases} \sqrt{1-4\pi\overline{v}(\boldsymbol{r})/K^2} & \text{for neutrons,} \\ \sqrt{\epsilon(\boldsymbol{r})} & \text{for X-rays.} \end{cases} \tag{1.28}$$ {EnkK}

If $\overline{v}(\boldsymbol{r})$ or $\epsilon(\boldsymbol{r})$ has an imaginary part, describing absorption, then $n(\boldsymbol{r})$ is a complex number. Conventionally, n is parameterized by two real numbers:

$$n =: 1-\delta+i\beta. \tag{1.29}$$ {Endb1}

Appendix A explains how to determine δ and β.

For thermal neutrons and X-rays, δ and β are almost always nonnegative,[8] and much smaller than 1. This explains why in most scattering geometries the ordinary Born approximation with $\boldsymbol{\Lambda} \equiv 0$ is perfectly adequate. In layered samples under grazing incidence, however, even small differences in n can cause substantial *refraction* and *reflection*. To model GISAS, therefore, it is necessary to use DWBA, and to let $\boldsymbol{\Lambda}$ represent the average vertical refractive index profile $\overline{n}(z)$.

1.2.3 Scattering cross section in DWBA

Altogether, we need to consider three different wave equations, which we write here in function-space notation: The vacuum wave equation that it solved by plane-wave states,

$$\boldsymbol{D}_0\,|\boldsymbol{k}\alpha\rangle = 0; \tag{1.30}$$ {EWave1}

the unperturbed distorted-wave equation (1.26),

$$\boldsymbol{D}\,|\boldsymbol{\Phi}\rangle = 0; \tag{1.31}$$ {EWave2}

and the wave equation (1.16) of the full, perturbed problem

$$(\boldsymbol{D}-\boldsymbol{U})\,|\boldsymbol{\Psi}\rangle = 0. \tag{1.32}$$ {EWave3}

To solve (1.32), we first transform it into a Lippmann-Schwinger equation,

$$|\boldsymbol{\Psi}\rangle = |\boldsymbol{\Phi}_\mathrm{i}\rangle + \boldsymbol{G}\boldsymbol{U}\,|\boldsymbol{\Psi}\rangle \tag{1.33}$$ {ELS3}

with the Green function

$$\boldsymbol{G} \coloneqq \boldsymbol{D}^{-1} \tag{1.34}$$ {EdefG}

and with the incident distorted wave $|\boldsymbol{\Phi}_\mathrm{i}\rangle$. To see that the left-hand side of (1.33) solves indeed the wave equation (1.32), operate from the left with $\boldsymbol{D}$ on both sides of (1.33).

[8] The plus sign in front of $i\beta$ is a consequence of the quantum-mechanical sign convention (1.2) and (1.11); in the X-ray crystallography convention it would be a minus sign.

The Lippmann-Schwinger equation can be resolved by iterative substitution into an infinite series,

$$|\Psi\rangle = |\Phi_\mathrm{i}\rangle + \boldsymbol{GU}\,|\Phi_\mathrm{i}\rangle + \boldsymbol{GUGU}\,|\Phi_\mathrm{i}\rangle + \ldots \tag{1.35}$$ {EBornSeries}

This is the *Born expansion* or *Born series*.[9] As long as $\boldsymbol{U}$ is a small perturbation, the series converges quickly. In *first-order Born approximation*, only the linear order in $\boldsymbol{U}$ is retained,

$$|\Psi\rangle = (1 + \boldsymbol{GU})\,|\Phi_\mathrm{i}\rangle\,. \tag{1.36}$$ {EBorn1}

In scattering experiments we are only interested in the scattered wave at positions $\boldsymbol{r}$ that are far away from the sample ($r \to \infty$) and that are not illuminated by the distorted (refracted or reflected) incident beam,

$$|\Psi_\mathrm{s}^\infty\rangle \coloneqq \boldsymbol{G}^\infty\boldsymbol{U}\,|\Phi_\mathrm{i}\rangle\,. \tag{1.37}$$ {EBornS}

This is the base for material investigations with X-rays or neutrons, where sample structures that modulate the perturbation potential $\boldsymbol{U}$ are deduced from the differential scattering cross section

$$\frac{\mathrm{d}\sigma}{\mathrm{d}\Omega} \coloneqq \frac{r^2 J_\mathrm{f}(\boldsymbol{r})}{J_\mathrm{i}} = r^2|\Psi_\mathrm{s}^\infty(\boldsymbol{r})|^2, \tag{1.38}$$ {Exsectiondef}

assuming that the incident wave Φ_i, excited by a plane wave $|\Phi_\mathrm{i}^\infty\rangle = |\boldsymbol{k}_\mathrm{e}\alpha_\mathrm{e}\rangle$, is normalized to unity, $|\Phi_\mathrm{i}^\infty|^2 = 1$.

1.2.4 The DWBA far-field Green function

From Sec. 1.2.3, the task is left over to determine the far-field Green function G^∞. Assume we know the Green function of the undistorted wave equation (1.30), $\boldsymbol{G}_0 \coloneqq \boldsymbol{D}_0^{-1}$. Write the distorted wave equation (1.31) as a Lippmann-Schwinger equation

$$|\Phi\rangle = |\boldsymbol{k}\alpha\rangle + \boldsymbol{G}_0\boldsymbol{U}\,|\Phi\rangle\,. \tag{1.39}$$ {ELS2}

To verify, operate with $\boldsymbol{D}_0$ from the left. Solve formally through simple algebraic manipulations,

$$|\Phi\rangle = (\boldsymbol{1} - \boldsymbol{G}_0\boldsymbol{U})^{-1}\,|\boldsymbol{k}\alpha\rangle =: \boldsymbol{R}\,|\boldsymbol{k}\alpha\rangle\,. \tag{1.40}$$ {EPhi}

DiWa84,DiWa85,DiWa16

Following Dietrich and Wagner [13, 14, 15], we note that the distorted-wave Green function (1.34) also obeys a Lippmann-Schwinger equation,

$$\boldsymbol{G} = \boldsymbol{G}_0 + \boldsymbol{G}_0\boldsymbol{U}\boldsymbol{G}. \tag{1.41}$$

[9] Named after Max Born who introduced it in quantum mechanics. It is actually due to Lord Rayleigh who devised it for sound, and later also applied it to electromagnetic waves, which resulted in his famous explanation of the blue sky.

To verify, operate again with $\boldsymbol{D}_0$ from the left. Resolve algebraically for

$$\boldsymbol{G} = (\mathbf{1} - \boldsymbol{G}_0\boldsymbol{U})^{-1}\boldsymbol{G}_0 =: \boldsymbol{R}\boldsymbol{G}_0. \tag{1.42}$$

To make use of (1.40), we insert a complete projector,

$$\boldsymbol{G} = \sum_\alpha \int \mathrm{d}^3k\, \boldsymbol{R}\,|\boldsymbol{k}\alpha\rangle\,\langle\boldsymbol{k}\alpha|\,\boldsymbol{G}_0 = \sum_\alpha \int \mathrm{d}^3k\; |\boldsymbol{\Phi}_{\boldsymbol{k}\alpha}\rangle\,\langle\boldsymbol{k}\alpha|\,\boldsymbol{G}_0 \tag{1.43}$$

where the dependence of $\boldsymbol{\Phi}$ on the boundary condition $\boldsymbol{k}\alpha$ is explicitly denoted. As $\boldsymbol{G}_0$ is known in real-space representation, we insert another projector,

$$\boldsymbol{G} = \sum_\alpha \int \mathrm{d}^3k \int \mathrm{d}^3r''\; |\boldsymbol{\Phi}_{\boldsymbol{k}\alpha}\rangle\,\langle\boldsymbol{k}\alpha|\boldsymbol{r}''\rangle\,\langle r''|\,\boldsymbol{G}_0. \tag{1.44}$$

In real-space coordinates,

$$\boldsymbol{G}(\boldsymbol{r},\boldsymbol{r}') = (2\pi)^{-3}\sum_\alpha \int \mathrm{d}^3k \int \mathrm{d}^3r''\, \boldsymbol{\Phi}_{\boldsymbol{k}\alpha}(\boldsymbol{r})\cdot\hat{\boldsymbol{u}}_\alpha \mathrm{e}^{-i\boldsymbol{k}\boldsymbol{r}''}\boldsymbol{G}_0(\boldsymbol{r}'',\boldsymbol{r}'). \tag{1.45}$$ {EGrspace}

At this point, we need the vacuum Green function $\boldsymbol{G}_0$. In the scalar case, for an outgoing wave, it is

$$G_0(\boldsymbol{r},\boldsymbol{r}') = \frac{\mathrm{e}^{iK|\boldsymbol{r}-\boldsymbol{r}'|}}{4\pi|\boldsymbol{r}-\boldsymbol{r}'|} =: g(|\boldsymbol{r}-\boldsymbol{r}'|). \tag{1.46}$$ {EGo1}

for polarized neutrons,

$$\boldsymbol{G}_0(\boldsymbol{r},\boldsymbol{r}') = \mathbf{1}G_0(\boldsymbol{r},\boldsymbol{r}'); \tag{1.47}$$ {EGo2}

for X-rays[10]

$$\boldsymbol{G}_0(\boldsymbol{r},\boldsymbol{r}') = (\mathbf{1} - K^{-2}\boldsymbol{\nabla}\cdot\boldsymbol{\nabla})G_0(\boldsymbol{r},\boldsymbol{r}'). \tag{1.48}$$ {EGo3}

The far-field limit is usually considered in the first argument,

$$\boldsymbol{G}_0^\infty(\boldsymbol{r},\boldsymbol{r}') \coloneqq \lim_{r\to\infty} \boldsymbol{G}_0(\boldsymbol{r},\boldsymbol{r}'), \tag{1.49}$$ {EGinftydef}

but it is easily seen from (1.46) to (1.48) that

$$\boldsymbol{G}_0(\boldsymbol{r},\boldsymbol{r}') = \boldsymbol{G}_0(\boldsymbol{r}',\boldsymbol{r}), \tag{1.50}$$ {EGoReci}

as expected from more general reciprocity theorems [16]. Pot04

We expand for $\boldsymbol{r}'$ with $r' \ll r$:

$$\left|\boldsymbol{r}-\boldsymbol{r}'\right| \doteq \sqrt{r^2 - 2\boldsymbol{r}\,\boldsymbol{r}'} \doteq r - \frac{\boldsymbol{r}\,\boldsymbol{r}'}{r} \equiv r - \frac{\boldsymbol{k}_\mathrm{f}\boldsymbol{r}'}{K}, \tag{1.51}$$

[10] Eqn. B5 of [13] has a sign error. Pie84

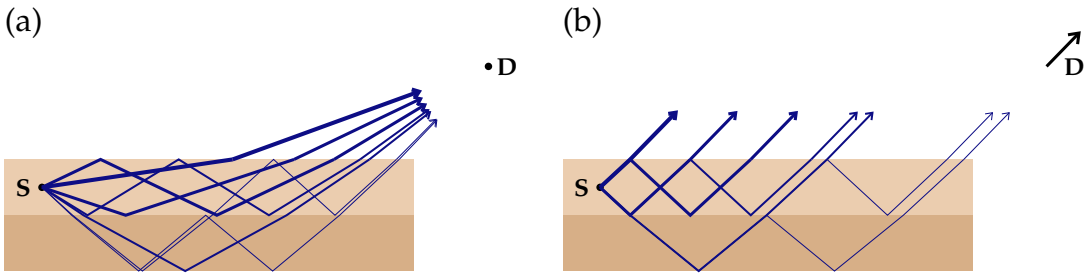

Figure 1.1: (a) The Green function $G(\boldsymbol{r}_\mathrm{S}, \boldsymbol{r}_\mathrm{D})$ is the probability that radiation emitted by a source S is reaches a detector D. If S is a locus of scattering in a multilayer sample, then G is a sum over different trajectories, involving refraction and reflection at layer interfaces. (b) For the far-field Green function $G^\infty(\boldsymbol{r}_\mathrm{S}, \boldsymbol{r}_\mathrm{D})$, the detector is moved so far away from the sample that all trajectories are practically parallel when they leave the sample.

where we have introduced the outgoing wavevector $\boldsymbol{k}_\mathrm{f} := K\boldsymbol{r}/r$. We apply this to (1.46), and obtain in leading order the far-field Green function

$$G_0^\infty(\boldsymbol{r}, \boldsymbol{r}') = g(r)\psi_\mathrm{f}^*(\boldsymbol{r}'), \tag{1.52}$$ {EGoFar1}

where g is the outgoing spherical wave introduced in (1.46),

$$\psi_\mathrm{f}(\boldsymbol{r}) := \mathrm{e}^{i\boldsymbol{k}_\mathrm{f}\boldsymbol{r}} \tag{1.53}$$

is a plane wave propagating towards the detector, and ψ^* designates the complex conjugate of ψ. The $\boldsymbol{\nabla}\cdot\boldsymbol{\nabla}$ term in (1.48) is negligible for $Kr \gg 1$, hence

$$\boldsymbol{G}_0^\infty(\boldsymbol{r}, \boldsymbol{r}') = \mathbf{1}G_0(\boldsymbol{r}, \boldsymbol{r}') \tag{1.54}$$ {EGoFar2}

in the polarized neutron as in the X-ray case. We apply reciprocity (1.50) to (1.52) and (1.54) and insert the resulting

$$\boldsymbol{G}_0^\infty(\boldsymbol{r}, \boldsymbol{r}') = \mathbf{1}\psi_\mathrm{f}^*(\boldsymbol{r})g(r') \tag{1.55}$$

into (1.45) to obtain

$$\lim_{r'\to\infty} \boldsymbol{G}(\boldsymbol{r}, \boldsymbol{r}') = \boldsymbol{\Phi}_{\boldsymbol{k}_\mathrm{f}\alpha}(\boldsymbol{r}) \cdot \hat{\boldsymbol{u}}_\alpha g(r'). \tag{1.56}$$ {EGresult}

1.2.5 Reciprocity of the Green function

Our computation of G_∞ will be based on a source-detector *reciprocity theorem* for the scalar Schrödinger equation.[11] The theorem states: Any Green function $G(\boldsymbol{r}, \boldsymbol{r}')$ that solves **??** and as function of $\boldsymbol{r}$ represents an outgoing wave is invariant under an exchange of source location $\boldsymbol{r}_\mathrm{S}$ and detection point $\boldsymbol{r}_\mathrm{D}$:

$$G(\boldsymbol{r}_\mathrm{S}, \boldsymbol{r}_\mathrm{D}) = G(\boldsymbol{r}_\mathrm{D}, \boldsymbol{r}_\mathrm{S}). \tag{1.57}$$ {Erecip}

[11] There exists a confusing multitude of reciprocity theorems [16]. In the end, we found it simpler to provide a derivation taylored for our application case than to refer to the literature.

Readers not interested in mathematical details may skip the following *proof*:

We introduce the auxiliary vector field

$$\boldsymbol{X}(\boldsymbol{r},\boldsymbol{r}_\mathrm{S},\boldsymbol{r}_\mathrm{D}) \coloneqq G(\boldsymbol{r},\boldsymbol{r}_\mathrm{D})\boldsymbol{\nabla}G(\boldsymbol{r},\boldsymbol{r}_\mathrm{S}) - G(\boldsymbol{r},\boldsymbol{r}_\mathrm{S})\boldsymbol{\nabla}G(\boldsymbol{r},\boldsymbol{r}_\mathrm{D}). \tag{1.58}$$

We inscribe the sample and the detector into a sphere $\mathcal{S}$ around the coordinate origin with radius R, and compute the volume integral

$$I(\boldsymbol{r}_\mathrm{S},\boldsymbol{r}_\mathrm{D}) \coloneqq \int_{\mathcal{S}} \mathrm{d}^3 r\, \boldsymbol{\nabla}\boldsymbol{X}(\boldsymbol{r},\boldsymbol{r}_\mathrm{S},\boldsymbol{r}_\mathrm{D}). \tag{1.59}$$ {Eprerecipro}

After a few steps, not entirely trivial, but not too difficult either, we obtain

$$I(\boldsymbol{r}_\mathrm{S},\boldsymbol{r}_\mathrm{D}) = G(\boldsymbol{r}_\mathrm{S},\boldsymbol{r}_\mathrm{D}) - G(\boldsymbol{r}_\mathrm{D},\boldsymbol{r}_\mathrm{S}). \tag{1.60}$$ {EIBD}

Alternatively, we can compute I as a surface integral

$$I(\boldsymbol{r}_\mathrm{S},\boldsymbol{r}_\mathrm{D}) = \int_{\partial\mathcal{S}} \mathrm{d}\boldsymbol{\sigma}\, \boldsymbol{X}(\boldsymbol{r},\boldsymbol{r}_\mathrm{S},\boldsymbol{r}_\mathrm{D}). \tag{1.61}$$

On the surface $\partial\mathcal{S}$, G is an outgoing solution of the Helmholtz equation. As such, it has a well-known series expansion in spherical coordinates. We send $R \to \infty$ so that we need only to retain the lowest order:

$$G(\boldsymbol{r}(R,\vartheta,\varphi),\boldsymbol{r}_\mathrm{D}) \doteq \frac{\mathrm{e}^{iKR}}{4\pi R} a(\vartheta,\varphi), \tag{1.62}$$

$$G(\boldsymbol{r}(R,\vartheta,\varphi),\boldsymbol{r}_\mathrm{S}) \doteq \frac{\mathrm{e}^{iKR}}{4\pi R} b(\vartheta,\varphi). \tag{1.63}$$

The factorization of G and B and their common R dependence imply that

$$I(\boldsymbol{r}_\mathrm{S},\boldsymbol{r}_\mathrm{D}) = \int_{\partial\mathcal{S}} \mathrm{d}\sigma\, (R\text{-dependent})(ab - ba) = 0. \tag{1.64}$$

Comparison with (1.60) yields (1.57), which completes the proof.

OLD STUFF

exciting vs incident wave

The solution of the wave equation **??** starts with the determination of the incident wave $\boldsymbol{\Psi}_\mathrm{i}$. It is important to distinguish the *incident* from the *exciting* wave. They coincide in ordinary Born approximation, but not in DWBA.

The *exciting wave* is prepared far outside the sample by a radiation source and some optical devices. It is a superposition of plane waves, as discussed later in the context of instrumental resolution effects (**??**). Here we will consider a single plane wave $\boldsymbol{\Psi}_\mathrm{e}(\boldsymbol{r}) = \hat{\boldsymbol{u}}_\mathrm{e} \mathrm{e}^{i\boldsymbol{k}_\mathrm{e}\boldsymbol{r}}$. This function is defined for all $\boldsymbol{r}$, but is physical only along the primary beam, upstream of the sample.

The *incident wave* $\boldsymbol{\Psi}_\mathrm{i}$ is an exact solution of (1.26) under the boundary condition that it match $\boldsymbol{\Psi}_\mathrm{e}$ upstream of the sample. Inside the sample it undergoes refraction and reflection or other modifications under the influence of the distortion field $\boldsymbol{\Lambda}$.

Scattering vector q

the *scattering vector*[12]

$$\boldsymbol{q} \coloneqq \boldsymbol{k}_\mathrm{f} - \boldsymbol{k}_\mathrm{i}. \tag{1.65}$$ {Eq}

[12] With this choice of sign, $\hbar\boldsymbol{q}$ is the momentum *gained* by the scattered neutron, and *lost* by the sample. In much of the literature the opposite convention is prefered, since it emphasizes the sample physics over the scattering experiment. However, when working with two-dimensional detectors it is highly desirable to express pixel coordinates and scattering vector components with respect to equally oriented coordinate axes, which can only be achieved by the convention (1.68).

1.3 Coherent vs incoherent scattering

1.3.1 Coherence length

Per **??** and **??**, the matrix element $\langle\psi_\mathrm{i}|\delta v|\psi_\mathrm{f}\rangle$ is given by a three-dimensional integral

$$\langle\psi_\mathrm{i}|\delta v|\psi_\mathrm{f}\rangle \coloneqq \int \mathrm{d}^3 r\, \psi_\mathrm{i}^*(\boldsymbol{r})\delta v(\boldsymbol{r})\psi_\mathrm{f}(\boldsymbol{r}). \tag{1.66}$$ {Etrama3}

The integration domain is effectively limited to a finite z interval, where $\delta v(\boldsymbol{r})$ is nonzero. The horizontal integration domain, however, is infinite within our formalism, which is of course an idealization. Obviously, physical integration limits are imposed by the finite *illuminated sample area*.[13] Another limitation comes from the finite *coherence length* of the instrumental setup, which usually is much shorter than the sample width and length [17, 18].[14] {HaPR10,MaMM14}

While each single neutron is described by a wavefunction that allows for *coherent* superposition of different contributions to the scattered wavefunction, the final detector statistics is given by an *incoherent* sum over the differential cross sections of individual neutrons. The finite *resolution* of an experimental setup is in part due to the fact that different neutrons have different wavenumbers, originate[15] at different points in the moderator, and are detected at slightly different points within one detector pixel. This can be modeled by computing expected scattering intensities as averages over different neutrons with K, $\hat{\boldsymbol{k}}_\mathrm{i}$, and $\hat{\boldsymbol{k}}_\mathrm{f}$ drawn at random from appropriate distributions.

However, this is not the full story. In the above introduction to the Born approximation we have made the standard assumption that an incoming neutron can be described by a plane wave $\psi_\mathrm{i} = \mathrm{e}^{i\boldsymbol{k}_\mathrm{i}\boldsymbol{r}}$. The wavefunction ψ_f traced back from the detector is also approximated by a plane wave. In the DWBA we allow these waves to be distorted within the sample, but when impinging on the sample they still are plane. A plane wave obviously is an idealized concept, since it has infinite lateral extension. The *transverse coherence length* indicates the scale beyond which this approximation becomes invalid. At larger scales, the wave fronts appear randomly distorted. Physical causes of these distortions include reflections in the neutron guide, diffraction by guide windows and other slits, and diffraction by imperfect monochromator crystals. Of course the distorted wave still admits a Fourier decomposition into plane waves with slightly different wavevectors. In practice, it is impossible to distinguish this spread of wavevectors from the incoherent spread described in the previous paragraph. The instrumental resolution function therefore accounts for both causes of wavevector distortion.

Usually, therefore, a GISANS image is an incoherent average over coherent diffraction patterns collected from many small subareas of the sample. Only horizontal sample

[13] We assume a well aligned instrument, for which the beam footprint and the backtracked detector footprint agree within reasonable accuracy.

[14] These two references also make clear that the theoretical description and the experimental determination of coherence lengths are difficult problems and subject of ongoing research.

[15] It is reasonable to take the last collision in the moderator as the *origin* of a neutron ray, since collisions between neutrons and hydrogen nuclei bound in disordered matter lead to almost perfect decoherence.

structures on scales smaller the coherence length yield interference patterns. Structure fluctuations on larger scales produce said incoherent average of different GISANS images.

The crossover from coherent to incoherent scattering is of course a gradual one. The coherence length indicates where a certain, somewhat arbitrary degree of decoherence is reached. Under these reservations one defines a *coherence spot* in the cross section of an approximately plane wave as an area where the coherence is above a certain threshold. Unless the wave has been prepared in a highly anisotropic guide and slit system, this spot is about circular. Under grazing incidence conditions however, the projection of this spot onto the sample surface yields a very elongated ellipse. Therefore, the coherence length is much larger in x than in y or z direction.[16]

1.3.2 Implementation

Unless otherwise said, BornAgain simulates *coherent* diffraction patterns obtained by the linear superposition of scattered waves. To simulate an *incoherent* mixture of diffraction patterns, the most generic solution is a script with an outer loop that averages over several coherent computations with appropriately distributed parameters.

Currently, BornAgain does not support interferences between particles in different layers.

[16] This has nothing to do with the distinction of *transverse* and *longitudinal* coherence length. Longitudinal coherence has to do with wavelength stability and is of no importance for elastic scattering. We are talking here about *horizontal* and *vertical* projections of the *transverse* coherence length.

A Refractive Indexes for Neutrons and X-Rays

A.1 Introduction

For both, neutrons and X-rays, the refractive index n is defined as (1.29)

$$n \equiv 1 - \delta + i\beta. \tag{A.1}$$

where δ and β are defined in a different way for neutrons and X-rays.

A.2 Calculation for neutrons

For unpolarized neutrons, δ and β are calculated in a following way [19]:

$$\delta = \frac{Nb\lambda^2}{2\pi}, \quad \beta = \frac{N\alpha_a\lambda}{4\pi} \tag{A.2}$$ {eq:deltabeta}

where N is the atomic number density, b is the coherent scattering length, λ is the neutron wavelength, α_a is the absorption cross-section. Nb is also called neutron scattering length density (SLD) and can be calculated using the online calculators. b and α_a are to be found in tables [20]. N is calculated as

$$N = \frac{N_a}{V} \tag{A.3}$$

where $N_a = 6.022 \times 10^{23}$ mol^{-1} is the Avogadro constant and V is the molar volume (cm^3/mol) evaluated as:

$$V = \frac{M}{\rho} \tag{A.4}$$

Here M is the molar mass (g/mol) of the material and ρ is the mass density (g/cm^3). It is important to mention, that for the complex materials, M, b and α_a are calculated as a sum of those for the compounds. α_a in the table [20] is given for the neutron velocity of 2200 m/s and must be recalculated for the considered λ. For this recalculation assumption that $\alpha_a \propto 1/v$, where v is the neutron velocity, is used. Since $v \propto 1/\lambda$, for the given wavelength one can use the following expression:

$$\alpha_a(\lambda) = \alpha_a(2200 \text{ m/s}) \cdot \frac{\lambda}{1.798} \tag{A.5}$$

where λ is the wavelength in Å and 1.798 Å is the wavelength corresponding to the neutron velocity of 2200 m/s.

Example. In the following example we calculate the δ and β for the GaAs using the aforementioned expressions. Molar masses can be taken from the periodic table.

$$\begin{aligned} M_{Ga} &= 69.723 \text{ g/mol} \\ M_{As} &= 74.921595 \text{ g/mol} \\ M_{GaAs} &= M_{Ga} + M_{As} \\ \rho_{GaAs} &= 5.32 \text{ g/cm}^3 \end{aligned}$$

Incoherent scattering lengths and absorption cross-sections are taken from the table [20].

$$\begin{aligned} b_{Ga} &= 7.288 \times 10^{-13} \text{ cm} \\ b_{As} &= 6.58 \times 10^{-13} \text{ cm} \\ b_{GaAs} &= b_{Ga} + b_{As} \\ \alpha_a(Ga) &= 2.75 \times 10^{-24} \text{ cm}^2 \\ \alpha_a(As) &= 4.5 \times 10^{-24} \text{ cm}^2 \\ \alpha_a(GaAs) &= \alpha_a(Ga) + \alpha_a(As) \end{aligned}$$

Let's consider that $\lambda = 12$ Å. For this wavelength, the $\alpha_a(GaAs)$ is recalculated as

$$\alpha_a(GaAs, 12 \text{ Å}) = \alpha_a(GaAs) \cdot \frac{12}{1.798} = 48.38179 \times 10^{-24} \text{ cm}^2$$

Finally, using these values in the equation (A.2), we obtain

$$\begin{aligned} \delta &= 7.04 \times 10^{-5} \\ \beta &= 1.0233 \times 10^{-8} \end{aligned}$$

Comment. For the case of absorption processes included, δ and β may be expressed in the following form [21]:

$$\delta = \frac{\lambda^2 N}{2\pi}\sqrt{b^2 - \left(\frac{\sigma_r}{2\lambda}\right)^2}, \qquad \beta = \frac{\sigma_r N \lambda}{4\pi} \tag{A.6}$$

where $\sigma_r = \alpha_a + \sigma_i$ is the sum of the absorption and incoherent scattering cross sections.

A.3 Case of polarized neutrons

For the spin-polarized neutrons scattered on the magnetic multilayers, the magnetic scattering length b_m must be taken into account. It can be expressed in the form [22]

$$b_m = 1.913 e^2 S / m_e \tag{A.7}$$

where S is the spin of the magnetic atom in the direction perpendicular to the momentum transfer $\mathbf{q}$ and e and m_e are the charge and mass, respectively, of the electron. The total coherent scattering length is then

$$b_{\text{total}} = b_{\text{nuclear}} \pm b_m \tag{A.8}$$

where the sign $\pm$ corresponds to the beam being polarized parallel or antiparallel to the magnetization direction of the sample [22]. Values for magnetic scattering lengths can be found in tables [23, 5, 21, 20, 24].

A.4 Calculation for X-rays

In the case of X-rays scattering originates from the strong variations of the mean electronic density as a homogeneous medium does not scatter [25]. Thus, the dispersion δ and absorption contribution β are expressed in the following form [25].

$$\delta(\mathbf{q},\lambda) = \frac{e^2\lambda^2}{8\pi^2 m_e c^2 \varepsilon_0} \cdot \rho \cdot \frac{\sum \left[f_k^0(\mathbf{q},\lambda) + f_k'(\lambda)\right]}{\sum M_k} \tag{A.9}$$

$$\beta = \frac{e^2\lambda^2}{8\pi^2 m_e c^2 \varepsilon_0} \cdot \rho \cdot \frac{\sum f_k''(\lambda)}{\sum M_k} \tag{A.10}$$

where c is the speed of light, ε_0 is the permittivity constant, M_k is the atomic weight of the atom k, and f_k' and f_k'' are the dispersion corrections [25] or atomic scattering factors [26]. The summation is performed over all compound atoms k. For the very high photon energies, f_k^0 approaches Z_k^*, which is expressed as [26]:

$$Z_k^* = Z_k - \left(\frac{Z_k}{82.5}\right)^{2.37} \tag{A.11}$$

where Z_k is the atomic number. Tables for the atomic scattering factors can be found in [26]. There are online calculators for the refractive indexes available in [27].

Bibliography

PoHB20 [1] G. Pospelov, W. Van Herck, J. Burle, J. M. Carmona Loaiza, C. Durniak, J. M. Fisher, M. Ganeva, D. Yurov and J. Wuttke, J. Appl. Cryst. **53**, 262 (2020). v, vi, 1:1, 1:2

Laz06 [2] R. Lazzari, *IsGISAXS*. Version 2.6. http://www.insp.jussieu.fr/oxydes/IsGISAXS/isgisaxs.htm (2006). vi

Laz02 [3] R. Lazzari, J. Appl. Cryst. **35**, 406 (2002). vi

ReLL09 [4] G. Renaud, R. Lazzari and F. Leroy, Surf. Sci. Rep. **64**, 255 (2009). vi, 1:3

Sea92 [5] V. P. Sears, Neutron News **3**, 26 (1992). 1:2, A:4, X:2

Sea89 [6] V. P. Sears, *Neutron Optics*, Oxford University Press: Oxford (1989). 1:2

Mez86 [7] F. Mezei, Physica B+C **137**, 295 (1986). 1:2

MaOB06 [8] C. F. Majkrzak, K. V. O'Donovan and N. F. Berk, in *Neutron Scattering from Magnetic Materials*, edited by T. Chatterji, Elsevier: Amsterdam (2006). 1:2

Lau31 [9] M. v. Laue, Erg. exakt Naturwiss. **10**, 133 (1931). 1:3

Sch14 [10] H. Schober, J. Neutron Res. **17**, 109 (2014). 1:6

Vin82 [11] G. H. Vineyard, Phys. Rev. B **26**, 4146 (1982). 1:6

MaMi82 [12] P. Mazur and D. L. Mills, Phys. Rev. B **26**, 5175 (1982). 1:6

DiWa84 [13] S. Dietrich and H. Wagner, Z. Phys. B **56**, 207 (1984). 1:6, 1:8, 1:9

DiWa85 [14] S. Dietrich and H. Wagner, Z. Phys. B **59**, 35 (1985). 1:6, 1:8

DiWa16 [15] S. Dietrich and H. Wagner, *Private communication* (2016). 1:8

Pot04 [16] R. J. Potton, Rep. Progr. Phys. **67**, 717 (2004). 1:9, 1:10

HaPR10 [17] V. O. de Haan, J. Plomp, M. T. Rekveldt, A. A. van Well, R. M. Dalgliesh, S. Langridge, A. J. Böttger and R. Hendrikx, Phys. Rev. B **81**, 094112 (2010). 1:13

MaMM14 [18] C. F. Majkrzak, C. Metting, B. B. Maranville, J. A. Dura, S. Satja, T. Udovic and N. F. Berk, Phys. Rev. A **89**, 033851 (2014). 1:13

Mue13 [19] P. Müller-Buschbaum, Polym. J. **45**, 34 (2013). A:2

2online [20] NIST Center for Neutron Research, *Neutron scattering lengths and cross sections according to [5]*, *http://www.ncnr.nist.gov/resources/n-lengths/list.html*. A:2, A:3, A:4

RaWa00 [21] H. Rauch and W. Waschkowski, in *Landolt-Börnstein - Group I Elementary Particles, Nuclei and Atoms 16A1 (Low Energy Neutrons and their Interaction with Nuclei and Matter. Part 1)*, edited by H. Schopper (2000). A:3, A:4, X:2

WiCa09 [22] B. T. M. Willis and C. J. Carlile, *Experimental neutron scattering*, Oxford University Press: Oxford (2009). A:4

KoRS91 [23] L. Koester, H. Rauch and E. Seymann, Atom. Data Nucl. Data **49**, 65 (1991). A:4, X:2

0online [24] Atominstitut der österreichischen Universitäten, *Neutron scattering lengths and cross sections according to [23, 21]*, *http://www.ati.ac.at/~neutropt/scattering/table.html*. A:4

Mue09 [25] P. Müller-Buschbaum, in *Applications of Synchrotron Light to Scattering and Diffraction in Materials and Life Sciences*, edited by M. Gomez, A. Nogales, M. C. Garcia-Gutierrez and T. A. Ezquerravolume 776 of *Lect. Notes Phys.* (Lect. Notes Phys. 776) (2009). A:5

HeGD93 [26] B. L. Henke, E. M. Gullikson and J. C. Davis, Atom. Data Nucl. Data **54**, 181 (1993). A:5, X:2

3online [27] Lawrence Berkeley National Laboratory, Materials Sciences Division, Center for X-Ray Optics, *X-Ray Interactions With Matter. Online calculators based on [26]*. *http://henke.lbl.gov/optical_constants*. A:5

List of Symbols

β	Imaginary part of the refractive index, 1:7
δ	Small parameter in the refractive index $n = 1 - \delta + i\beta$, 1:7
ϵ_0	Vacuum permittivity, 8.854…As/Vm, 1:3
$\epsilon(\boldsymbol{r})$	Relative dielectric permittivity function, 1:3
$\boldsymbol{\epsilon}(\boldsymbol{r})$	Relative dielectric permittivity tensor, 1:3
$\boldsymbol{\Lambda}(\boldsymbol{r})$	Distortion field, 1:6
μ_0	Vacuum permeability, $4\pi \cdot 10^{-7}$ Vs/Am, 1:2
μ_n	Magnetic moment of the neutron, 1:2
$\boldsymbol{\mu}(\boldsymbol{r})$	Relative magnetic permeability tensor, 1:3
$\hat{\rho}$	Density operator, 1:4
$\rho(\boldsymbol{r})$	Electron number density, 1:3
ρ_s	Number density of chemical element s, 1:2
σ	Scattering or absorption cross section, 1:12
$\boldsymbol{\sigma}$	Pauli vector, composed of the three Pauli matrices: $\boldsymbol{\sigma} = (\sigma_x, \sigma_y, \sigma_z)$, 1:2
$\psi(\boldsymbol{r})$	Stationary wavefunction, 1:1
$\psi(\boldsymbol{r}, t)$	Microscopic neutron wavefunction, 1:1
$\psi_\mathrm{f}(\boldsymbol{r})$	Plane wave propagating from the sample towards the detector, 1:15
$\psi_\mathrm{s}(\boldsymbol{r})$	Scattered wavefunction, 1:8
$\psi_{\mathrm{s}\infty}(\boldsymbol{r})$	Far-field approximation to the scattered wavefunction $\psi_\mathrm{s}(\boldsymbol{r})$, 1:15
$\boldsymbol{\Psi}_\mathrm{i}(\boldsymbol{r})$	Incident wavefunction, 1:8
$\boldsymbol{\Psi}_\mathrm{e}(\boldsymbol{r})$	Exciting wave, 1:8
$\boldsymbol{\Psi}(\boldsymbol{r})$	Generic wave amplitude, possibly vectorial or spinorial, 1:4

$\boldsymbol{\Psi}(\boldsymbol{r})$	Stationary coherent spinor wavefunction, 1:2
ω	Frequency of incident radiation, 1:1
Ω	Solid angle, 1:12
b	Bound scattering length, 1:2
$\boldsymbol{B}(\boldsymbol{r},t)$	Magnetic field, 1:3
$\boldsymbol{D}_0(\boldsymbol{r})$	Differential operator in the vacuum wave equation, 1:4
$\boldsymbol{D}(\boldsymbol{r})$	Differential operator in the wave equation, 1:6
$\boldsymbol{D}(\boldsymbol{r},t)$	Displacement field, 1:3
$\boldsymbol{E}(\boldsymbol{r},t)$	Electric field, 1:3
f	Subscript "final", 1:9
f	Subscript "final", 1:15
$\boldsymbol{G}(\boldsymbol{r},\boldsymbol{r}')$	Generic (possibly tensorial) Green function, 1:8
$\boldsymbol{G}^{\infty}(\boldsymbol{r},\boldsymbol{r}')$	Far-field approximation to the Green function $G(\boldsymbol{r},\boldsymbol{r}')$, 1:9
$\boldsymbol{b}(\boldsymbol{r})$	Rescaled field $\boldsymbol{b} = (m\mu/2\pi\hbar^2)\boldsymbol{B}$, 1:2
$\boldsymbol{B}(\boldsymbol{r},t)$	Magnetic induction, 1:2
i	Subscript "incident", 1:8
$\boldsymbol{J}(\boldsymbol{r})$	Flux, 1:5
$\boldsymbol{k}$	Wavevector, 1:4
K	Wavenumber in vacuum, 1:1
n	Refractive index, 1:7
$p_{\boldsymbol{k}\alpha}$	Weight of state $ket\boldsymbol{k}\alpha$ in the density operator, 1:4
$\boldsymbol{q}$	Scattering vector, 1:15
r_e	Classical electron radius $2.817\ldots^{-15}$ m, 1:3
$\boldsymbol{r}$	Position, 1:1
$\boldsymbol{r}_{\mathrm{D}}$	Position of detector, 1:11
$\boldsymbol{r}_{\mathrm{D}}$	Position of source, locus of scattering, 1:11
s	Subscript "scattered", 1:8
$\boldsymbol{S}$	Poyinting vector, 1:5

t	Time, 1:1
$\boldsymbol{U}(\boldsymbol{r})$	Perturbation potential, 1:6
$v(\boldsymbol{q})$	Fourier transform of the SLD $\delta v(\boldsymbol{r})$, 1:15
$v(\boldsymbol{r})$	Rescaled neutron potential, scattering length density (SLD), 1:2
$V(\boldsymbol{r})$	Neutron potential, 1:1
$\boldsymbol{V}(\boldsymbol{r})$	Generic potential, 1:4

Index